Journal of Hazardous Materials 181 (2010) 609–616

Contents lists available at ScienceDirect

Journal of Hazardous Materials

journal homepage: www.elsevier.com/locate/jhazmat

A numerical study of the evolution of the blast wave shape in tunnels

Adel M. Benselama[a,b,*], Mame J.-P. William-Louis[a,b], François Monnoyer[a,b], Christophe Proust[c]

[a] Univ Lille Nord de France, F-59000 Lille, France
[b] UVHC, LME, F-59313 Valenciennes, France
[c] Institut National de l'Environnement Industriel et des Risques, F-60550 Verneuil-en-Halatte, France

ARTICLE INFO

Article history:
Received 25 March 2010
Received in revised form 12 May 2010
Accepted 12 May 2010
Available online 25 May 2010

PACS:
47.40.Rs

Keywords:
Damage assessment for explosions
Three-dimensional simulation
Blast wave
Confined domain

ABSTRACT

When the explosion of condensed materials occurs in a tunnel, the subsequent blast wave reveals two patterns. The region close to the explosive charge exhibits a free-field overpressure decay pattern and the region far from the explosion, which undergoes much less overpressure decay, exhibits a quasi-one-dimensional pattern. Well-known overpressure decay laws that are applicable in each region already exist. In order to assess the validity range of each of these laws, the blast wave due an explosion inside a typical confined geometry is examined in order to determine the position of the transition zone from the free pattern to the one-dimensional pattern. To this end, the detonation of different quantities of explosive charges was simulated inside a tunnel with a constant cross-sectional area, and the wave aspect was determined for each region. This paper proposes a correlation law that defines the transition distance according to the explosive charge's weight and material and the geometry of the propagating domain. The validity of the proposed correlation law is corroborated by experimental results. In the authors' opinion, this law may be helpful for rapidly and efficiently drawing up the blast wave damage map.

1. Introduction

In order to assess the potential for damage and risk for both human and environmental factors, there are two propagation patterns that allow the overpressure experienced to be linked to the distance from the explosive charge in a straightforward manner. The first propagation pattern is the free-field case, which considers that the blast wave propagates freely in the atmosphere. Using the Sachs scaling law, Baker [1], Mills [2], Brode [3] and Henrych [4] have proposed general and equivalent fitting laws that relate the maximum overpressure peak to the distance from the explosive charge. In fact, Henrych [4] proposed one of the most common free-field decay law, which is expressed as follows:

$$\begin{cases} \dfrac{\Delta P_{max}}{P_{ref}}|_{Henrych} = \dfrac{14.072}{Z} + \dfrac{5.54}{Z^2} - \dfrac{0.357}{Z^3} + \dfrac{0.00625}{Z^4} & \text{if} \quad 0.05 \le Z \le 0.3 \\ \dfrac{\Delta P_{max}}{P_{ref}}|_{Henrych} = \dfrac{6.194}{Z} - \dfrac{0.326}{Z^2} + \dfrac{2.132}{Z^3} & \text{if} \quad 0.3 \le Z \le 1 \\ \dfrac{\Delta P_{max}}{P_{ref}}|_{Henrych} = \dfrac{0.662}{Z} + \dfrac{4.05}{Z^2} + \dfrac{3.288}{Z^3} & \text{if} \quad 1 \le Z. \end{cases} \tag{1}$$

In partially congested domains, the free-field propagation assumption leads to underestimating the overpressure and thus underestimating possible human casualties and structural damage.

The second propagation pattern is the case of a confined explosion, which considers that the blast wave propagates inside a confined space that is strong enough to withstand the explosive charge impulse (*e.g.* a tunnel). The shock wave attenuates, first, due to the rarefaction wave that degrades the front and, second, due to the interaction between the moving gas and the confining tunnel walls. Away from the explosive source, the maximum overpressure peak decreases mainly because of wall friction. Tunnel wall friction attenuates the blast wave to varying degrees, depending on the blast wavelength and velocity, time duration and the tunnel's cross-sectional area, roughness, gas density and viscosity.

Unlike free and surface blast propagation, very few experiments investigating air detonation in underground environments have been reported, mainly due to their military relevance. Taylor [5] presents a general overview of blast wave behavior in confined spaces. In Taylor's overview, the structural design of fuel and explosive storage in tunnels, chambers and tunnel junctions were specifically emphasized. Based on the results from experiments involving detonations at the closed-end of a tunnel, Curran [6] proposed the following pressure–distance law for various explosives weights:

$$\frac{\Delta p}{p_0} = \left(\frac{M}{\Phi^2 x}\right)^{0.8}. \tag{2}$$

In Curran's results, the peak overpressures ranged from 3.5 to 70 bar.

* Corresponding author at: UVHC, LME, F-59313 Valenciennes, France. Tel.: +33 327511971; fax: +33 327511961.
E-mail address: MustaphaAdel.Benselama@univ-valenciennes.fr (A.M. Benselama).

0304-3894/$ – see front matter © 2010 Elsevier B.V. All rights reserved.
doi:10.1016/j.jhazmat.2010.05.056

Nomenclature

Greek letters

α	ratio of the explosive diameter to the tunnel's hydraulic diameter $\alpha = 100 \times d/d_H$
Δx	mesh cell size (m)
Λ	length of the tunnel (m)
λ	mesh wavenumber, $\lambda = m_c^{1/3}/\Delta x$ (kg$^{1/3}$/m)
ω	constant for Jones–Wilkins–Lee (JWL) equation of state
Φ	tunnel cross-section diameter (m)
ρ	density (kg/m^3)

Latin letters

A	tunnel cross-sectional area (m^2)
A, B, C, R_1, R_2	constants for the JWL equation of state
d	explosive charge diameter (m)
d_H	hydraulic diameter of the tunnel (m)
E	total specific internal energy, $E = e + (1/2)(u^2 + v^2 + w^2)$ (J/kg)
e	specific internal energy (J/kg)
M	Mach number
m	weight (kg)
p	pressure (Pa)
r	radial coordinate (m)
T	total simulation time (s)
t	time (s)
x	distance from the blast source (m)
Z	reduced distance, $Z = x/m_c^{1/3}$ (m/kg$^{1/3}$)

Indices

0	reference conditions
c	explosive charge
H	hydraulic
Trans	transition

Smith et al. [7] investigated the applicability of Sachs' scaling law to explosions in confined spaces for overpressures up to 0.4 bar. For an explosion inside a tunnel that is closed at one end, these authors determined the following overpressure–distance decay relationship:

$$\frac{\Delta p}{p_0} = 7.028\left(\frac{M}{Ax}\right)^{0.514}. \tag{3}$$

Applying the energy concentration concept, Silvestrini et al. [8] proposed to extend the well-known free-field decay laws to confined spaces by modifying the evaluation distance. Instead of the regular reduced distance Z, these authors used the corrected reduced distance Z' in the free-field law (1). This corrected reduced distance Z' can be expressed as:

$$\frac{Z'}{Z} = \frac{1}{\left(V_{HSph}/V_{Tun}\right)^{1/3}}, \tag{4}$$

where V_{HSph}/V_{Tun} is the ratio of the hemisphere volume (with a radius equal to current distance x) to the volume of the tunnel portion extending to a distance equal to x. This ratio defines the energy concentration factor [8].

Fig. 1 shows the overpressure decay laws for the free and driven blast waves due to the detonation of 1 kg of TNT inside a tunnel with 1 m^2 cross-sectional area. The free decay law describes the explosion onset while the driven decay law describes the established one-dimensional blast wave inside the tunnel.

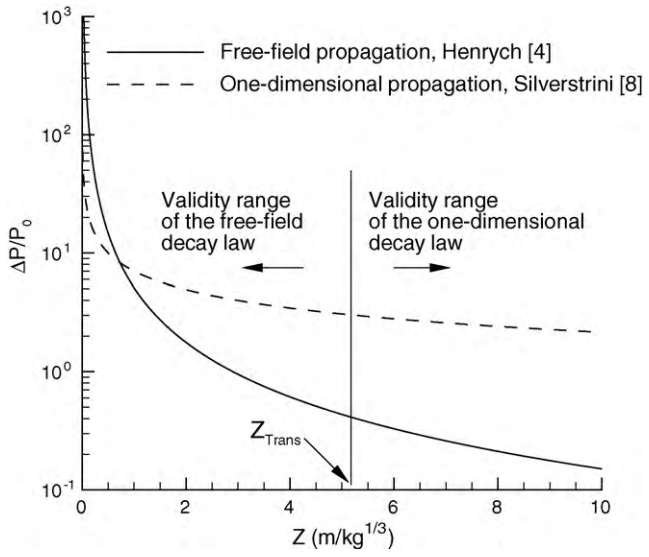

Fig. 1. The free-field and one-dimensional decay law. TNT explosive weight m_c = 1 kg and tunnel cross-sectional area A = 1 m^2.

Since the incident waves are spherical in source-explosions, the consequent reflections off the tunnel walls are generally due to oblique incident waves. Many theoretical and experimental studies of oblique shock waves have already been done. For instance, Baker et al. [1] and Kinney [9] have finely described the process of reflection. Fig. 2 shows an incident angle θ. As θ gets larger, the reflected wave can no longer maintain the flow near the wall parallel to the wall. As a result, the incident (Fig. 2(a)) and reflected (Fig. 2(b)) waves coalesce and form a third shock wave that is detached from the wall, called the Mach shock wave reflection (Fig. 2(c)). Stronger, the Mach shock wave reflection travels faster than the incident wave. The distance between the wall and the triple point, at which the incident, reflected and Mach waves join, grows as the shock system moves along the wall. In the case of spherical shock waves, whose strength is diminishing, the locus of the triple point curves away from the wall [10,11].

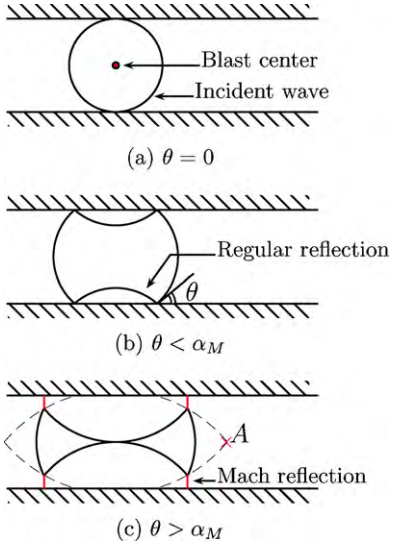

Fig. 2. Illustration of the wall reflections according to the blast wave incident angle θ: (a) incident wave, (b) regular reflection, and (c) Mach reflection.

Table 1
Parameters used for the JWL law describing the TNT explosive material.

Specific energy, e_c (kJ/kg)	Density, ρ_c (kg/m^3)	A ($\times 10^{11}$ Pa)	B ($\times 10^9$ Pa)	R_1	R_2	ω
4870	1580	3.73	3.74	4.15	0.90	0.35

Kinney [9] calculated the incident angle α_M at which the Mach reflection happens:

$$\alpha_M = \frac{35}{36}\frac{1}{M-1} + \frac{13}{60} \quad \text{for} \quad (M > 1). \tag{5}$$

When the angle θ is less than α_M, no Mach reflection is possible, thus the reflection is regular, as shown in Fig. 2. When the Mach reflections from each side of the tunnel coalesce at point A, as illustrated in Fig. 2(c), the whole tunnel cross-section is subjected to the same pressure signature. Thus, the position of point A may be considered as the transition zone from the freely-propagating blast wave to the one-dimensional blast wave propagating inside tunnels.

The objective of this paper is to determine the position of this transition zone. To accomplish this, the detonation of different quantities of TNT explosives inside a perfectly rigid tunnel was simulated. A scaling law that eliminates the solution's parametric dependence on the explosive energy, the weight of the explosives and the real tunnel cross-sectional size is provided. This scaling law transforms the infinite number of solutions into a single solution that demonstrates a monotonic transition from one wave pattern to the other. A fitting power law is proposed; in order to examine this law's validity, experimental data is compared to the results of the present simulation.

2. The configuration

In the present simulated configurations, different weights of a TNT explosive charge were located on the symmetry axis of a tunnel with a fixed square cross-sectional area. The TNT gases, composed of hot detonation products, obey the Jones–Wilkins–Lee law, which is expressed as [12]:

$$p = A\left(1 - \frac{\omega}{R_1}\frac{\rho}{\rho_c}\right)\exp\left(\frac{-R_1\rho_c}{\rho}\right) + B\left(1 - \frac{\omega}{R_2}\frac{\rho}{\rho_c}\right) \times \exp\left(\frac{-R_2\rho_c}{\rho}\right) + \omega\rho e, \tag{6}$$

where the parameters A, B, R_1, R_2, ω and ρ_c depend on the explosive material. Table 1 provides these parameters.

Because of the symmetry of the configuration, only one half of the blast charge propagating domain is considered here. The tunnel length is $\Lambda = 30$ m and its hydraulic diameter is $d_H = 5$ m. A series of gauges is located along the tunnel's symmetry axis and another one is located 2 m off-set from this axis. The successive gauges are separated by 1 m each, as illustrated in Fig. 3. In each series, the gauges are numbered from 1, the gauge nearest to the explosive charge, to 30, the gauge farthest from the explosive charge. As summarized in Table 2, six explosive charges were used. Each explosive weight corresponds to a parameter α, given by:

$$\alpha = 100\frac{d}{d_H}. \tag{7}$$

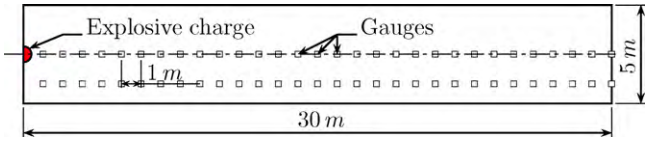

Fig. 3. Illustration of the configuration used to perform the parametric study.

Table 2
Explosive charges used in the present parametric study.

Weight (kg)	Diameter d ($\times 10^{-2}$ m)	Ratio size α	λ (m/kg$^{1/3}$)
0.150	5.687	1.14	78.0
0.300	7.16	1.43	98.7
1.000	10.7	2.14	142.2
5.000	18.3	3.66	242.8
10.000	23.05	4.61	306.3
15.000	26.39	5.28	350.6

Blast wave propagation is governed by the unsteady Euler equations, which were solved by a software developed in-house [13]. The numerical method on which this software's solver is based is a unstructured finite-volume cell-centered approach using the traditional upwind scheme and a two-stage explicit time integration technique, yielding an accuracy of the second-order in both space and time. In order to prevent numerical oscillations, which may occur in regions with strong gradients, the Total Variation Diminishing (TVD) minmod scheme was used [14]. The spatial discretization was performed with an automatic Cartesian grid generator [15]. In addition, the Courant–Friedrichs–Lewy (CFL) condition has to be satisfied in order to guarantee the stability of the time integration technique.

The propagation domain was split into approximately 5.8 million cells. The region near the explosion was more refined than the region farther from the explosion. On a computer with a 2.4 GHz CPU and 16 GB of memory, the simulation was performed up to 100 ms after the detonation, which took about 180 h for all the explosive charges tested. The values of the mesh wavenumber λ, which in the ideal case have to satisfy $\lambda > 100$ [13], are summarized in Table 2.

3. Results and discussion

Fig. 4 represents the blast wave arrival time versus the gauge position. The arrival time corresponds to the time elapsed between the detonation of the explosive and the wave passing by the series of gauges. Clearly, the larger the explosive charge, the smaller the arrival time. In addition, the distance variations for the farther

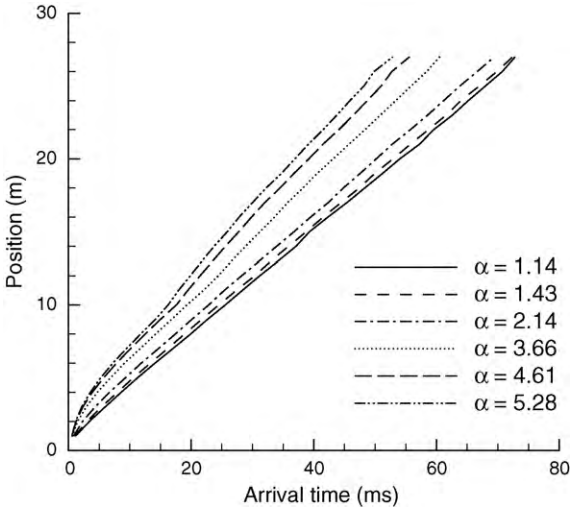

Fig. 4. Variations of the blast wave arrival time for the different explosive charges.

gauges seem to be practically linear with respect to the arrival time. The nonlinear variations are confined to the region close to the explosive charge. This linear behavior is more noticeable in Fig. 5(a) and (b) in which the propagating velocity, computed from the distance, is represented versus the distance and the reduced distance. Although some oscillations persist above the near-to-the-explosive-charge region, the velocity approaches an asymptotic constant value as the distance gets larger. The tendency toward the asymptotic value is more likely to happen closer to the explosive charge, when the weight of the charge is smaller.

In Fig. 6, the distribution of the maximum overpressure peak is represented versus the reduced distance Z recorded by the successive gauges inside the tunnel for each explosive charge weight. A spatial discontinuity in the maximum overpressure peak occurred for all tested explosive charges. As shown in Fig. 7, this discontinuity occurs at the same distance for the near-to-wall gauges, and thus corresponds to the Mach reflection of the incident blast wave on the tunnel walls. This Mach reflection is stronger and faster than the incident wave that generates it [1,10].

Apart from the purely geometric reasons, it may be possible to explain why the discontinuity occurs at longer distance for smaller quantities of explosives than for larger quantities as follows. As shown in Fig. 5(a), the smaller explosive charges generate a more moderate blast wave velocity, and thus the Mach number is more moderate. Consequently, according to Eq. (5), the Mach reflection, which determines the overpressure jump, happens at a larger angle α_M than for larger quantities of explosives. This larger angle α_M corresponds to a shift toward the upstream region of the Mach reflection.

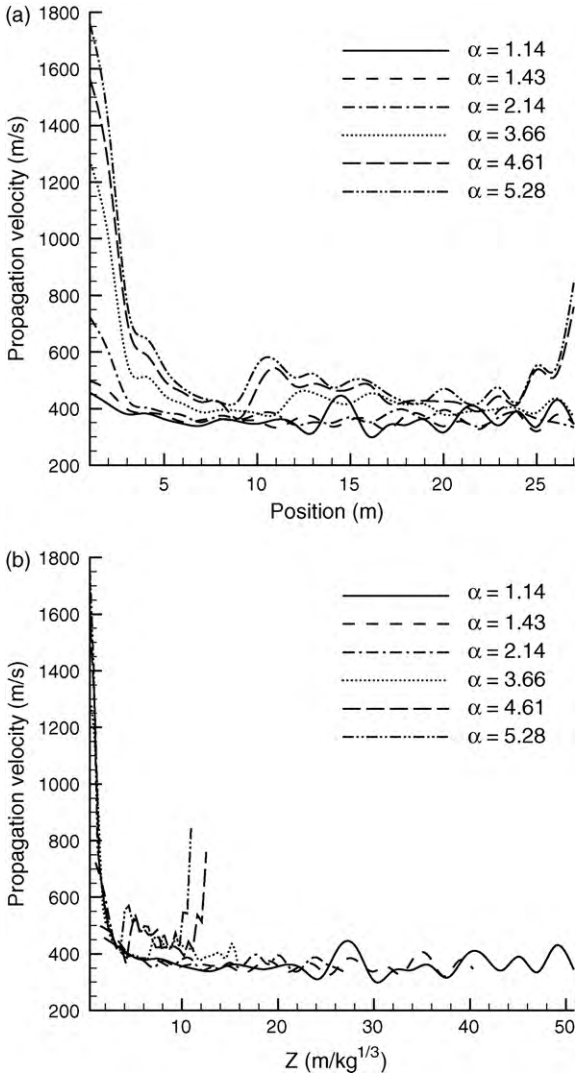

Fig. 5. Variations of the blast wave velocity for the different explosive charges: (a) versus the distance and (b) versus the reduced distance.

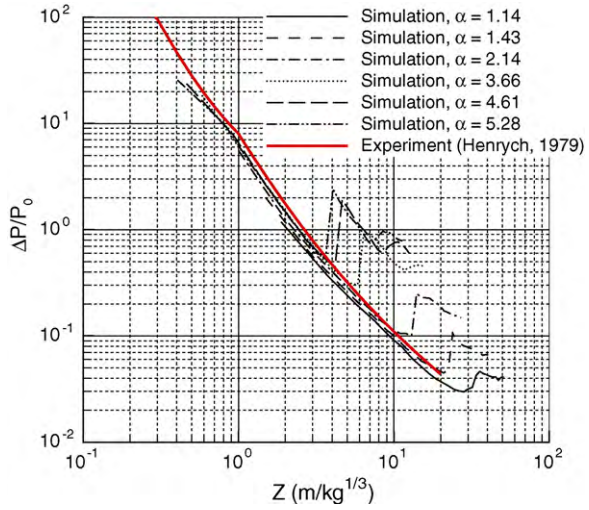

Fig. 6. Distribution of the maximum overpressure peak over the axial gauges for the different explosive charges.

Between the explosive charge and the location of the discontinuity, the maximum overpressure peak rapidly decreases with the reduced distance, whereas the decrease is smaller behind that discontinuity. In fact, in the region near the explosive charge, the maximum overpressure peak practically follows the free-field law in contrast with the region that is behind the discontinuity, where the decrease diverges from the free-field law and tends toward the constant law that characterizes the one-dimensional propagation pattern. It is thus reasonable to conclude that the location of the discontinuity determines the position of the transition zone where the wave propagation is transformed from free to one-dimensional behavior.

Fig. 8 shows the distribution of the Mach number at the middle of the tunnel's cross-section, as the time varies from 1 to 50 ms for the explosive charges $m_c = 0.300$ kg and $m_c = 5.000$ kg, respectively. The fact that the Mach reflection wave travels faster than

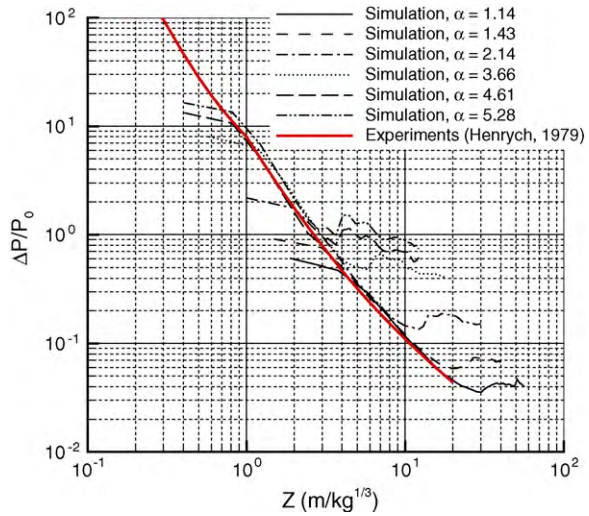

Fig. 7. Distribution of the maximum peak overpressure peak over the off-set gauges for the different explosive charges.

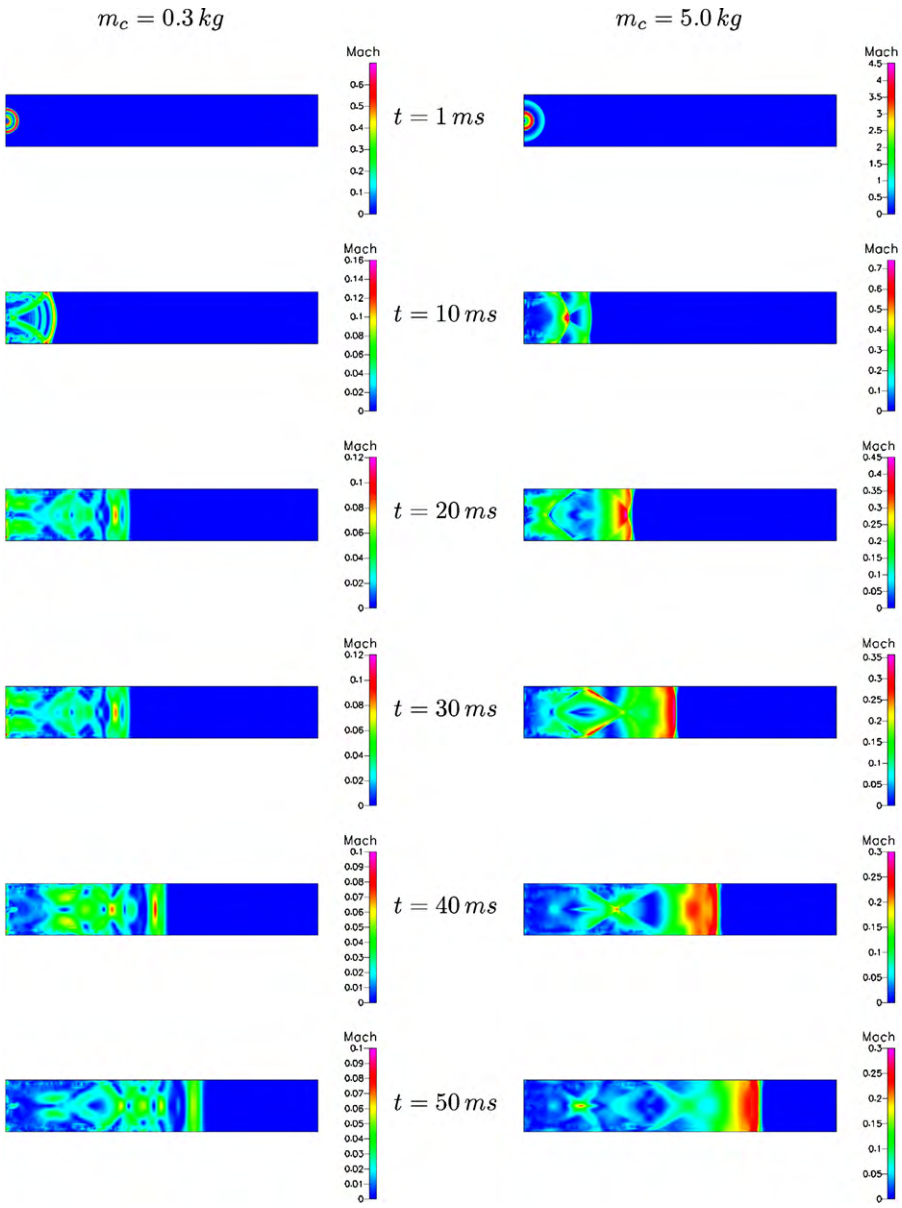

Fig. 8. Distribution of the Mach number at different times: (left) $m_c = 0.300$ kg; (right) $m_c = 5.000$ kg.

the incident wave is clearly distinguishable in these spanshots, which explains why the zone in which the three waves join together grows along the tunnel wall. The straight Mach reflection defines the region where the wave travels in a one-dimensional fashion.

Fig. 9 shows the variations of the discontinuity location Z_{Trans} versus the parameter α. Clearly, the correlation between the discontinuity location and the relative diameter of the explosives suggests a good fit with power-law. Using the traditional least square algorithm, the following fitting law can be deduced:

$$Z_{Trans} = \frac{0.0509}{\left(\alpha/100\right)^{13/9}}. \tag{8}$$

The fit has a correlation coefficient of 0.9436.

So in order to conveniently calculate the pressure level due to an explosion in a tunnel-like geometry, the steps below may be followed in succession:

- determine the quantity and the material of the explosives and the tunnel's characteristic hydraulic diameter;
- deduce the value of Z_{Trans} using Eq. (8);
- determine the reduced distance Z corresponding to the position at which the pressure level has to be evaluated; and
- apply the free-field pressure law, *i.e.* Eq. (1), if $Z < Z_{Trans}$, or the one-dimensional law, *i.e.* Eq. (1) combined with Eq. (4), if $Z > Z_{Trans}$.

This method could be very useful for assessing with relative good accuracy the pressure undergone, and thus the damage level provoked by an explosion inside a tunnel, provided that the quantity and the material of the explosives and the tunnel's characteristic cross-sectional area are known.

4. An extension for non-centered blast charges

The formula (8) is valid only when the explosive is located at mid-distance from the tunnel walls. When the explosive is near the tunnel wall, as shown in Fig. 10(a), the transition zone may vary from the case in which the explosive is centered. However, this "near" configuration may be easily transposed to the cen-

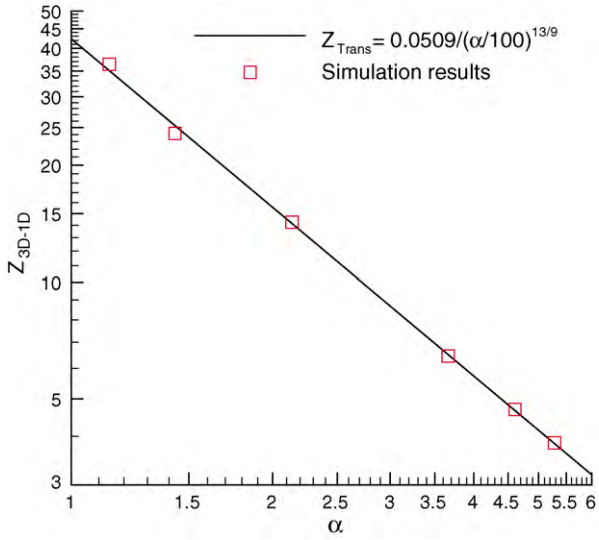

Fig. 9. Distribution of the reduced distance versus the relative size of the explosive charge.

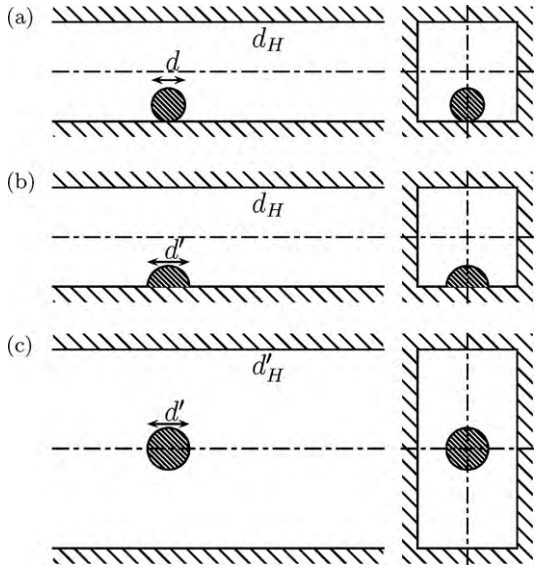

Fig. 10. The explosion configurations: (a) full-sphere near the tunnel wall, (b) half-sphere near the tunnel wall, and (c) centered equivalent sphere.

tered configuration as explained below. In fact, if the tunnel walls are assumed to be perfectly rigid, then the blast wave would be reflected back with small energy loss. This may be seen as the blast wave generated by a half sphere detonated on the ground

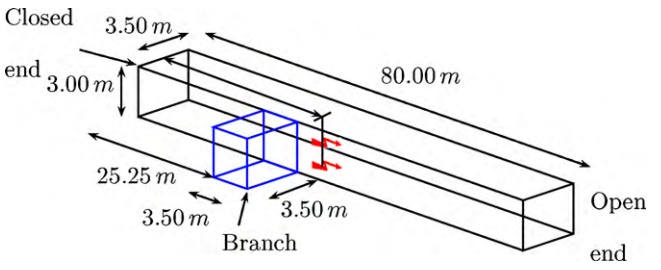

Fig. 12. Illustration of the tunnel configuration used in the INERIS experiments. The symbol indicates the position of the explosive.

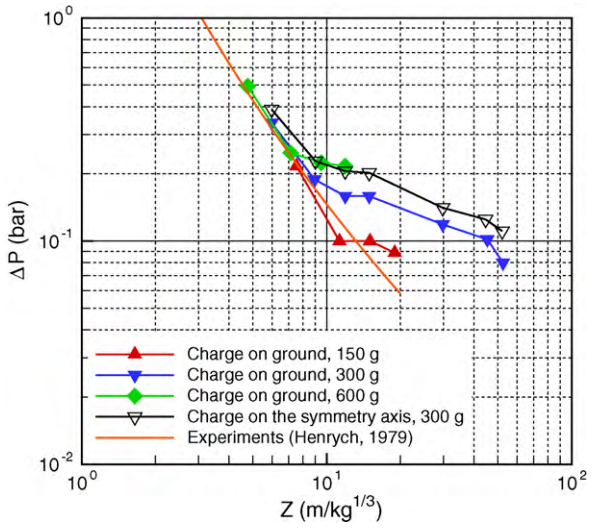

Fig. 13. Distribution of the measured maximum overpressure peak versus the reduced distance Z according to the INERIS and Henrych [4] experiments.

with the same weight of the original explosive charge, as shown in Fig. 10(b). If the ground or solid walls dissipate some of the energy, for instance, by cratering or in-structure shocks, a fairly correct rule requiring the quantity of explosives to be multiplied by a factor of $\beta = 1.8$ may be used [1]. Since the wall, near which the explosive is located, acts as a perfect reflecting surface, the blast wave would propagate similarly to the case in which the explosive is located at the axis of a new tunnel with a doubled height, as shown in Fig. 10(c).

With these pure geometric considerations, Eq. (8) may still be used provided that d is replaced by $d' = \sqrt[3]{\beta}d$ and d_H by $d'_H = 4/3d_H$. This is equivalent to applying a correction factor

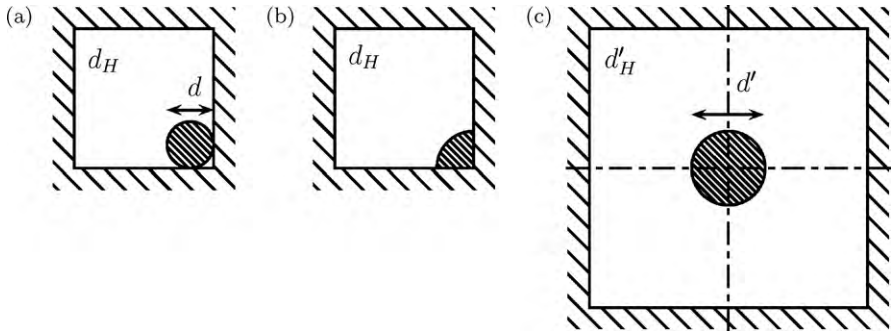

Fig. 11. The explosion configurations: (a) near the tunnel corner, (b) exactly at the tunnel corner, and (c) centered equivalent sphere.

Table 3
Comparison of the predicted transition distance of the Z_{Trans} and experimental results for an *NP*91 explosion.

Trial number	Configuration	Experimental range	Predicted value
1	150 *g* at ground level	15.50–19.05	18.48
2	300 *g* at ground level	12.01–15.22	13.25
3	600 *g* at ground level	7.19–10.56	9.47
4	300 *g* on the symmetry axis	8.96–12.00	11.60

Table 4
Comparison of the predicted and experimental values of the maximum overpressure peaks $\Delta p_{max}/p_0$ for Trial no. 2.

Z	Experimental $\frac{\Delta p_{max}}{p_0}$	Predicted $\frac{\Delta p_{max}}{p_0}$	Error %	Propagation pattern
6.03	0.3332	0.3140	−5.76	Free-field
9.017	0.1878	0.1700	−9.47	Free-field
15.22	0.1584	0.1885	19.00	One-dimensional
29.68	0.1189	0.1381	16.14	One-dimensional
45.28	0.1017	0.1107	8.85	One-dimensional

$\left((4/3)/\sqrt[3]{\beta}\right)^{13/9}$ to Eq. (8). Since this factor is greater than 1, β being at most equal to 2 [1], the reduced distance Z_{Trans} for an on-ground explosion would be larger than for an explosion in the center of the tunnel with the same quantity of explosives. Bearing in mind that the overpressure level decays with respect to Z, this also implies that the overpressure in the one-dimensional propagation region is smaller in the farther regions if the explosive charge is on the ground level than for the centered case.

An equivalent reasoning is valid if the explosive charge is located at the right corner of the tunnel. In that case, it may be easily derived that Eq. (8) holds if d is replaced by $d' = \sqrt[3]{\beta^2}d$ and d_H by $d'_H = 2d_H$, shown in Fig. 11. Hence, the correction factor is $\left(2/\sqrt[3]{\beta^2}\right)^{13/9}$ in order to take into account Eq. (8) for an on-the-corner explosion.

5. Validation of the model

In this section, the transition model from free-field to one-dimensional propagation deduced from this parametric study is validated by comparing the present simulation results with experimental data.

The available results are from a series of trials done by INERIS (French Institute of Industrial Environment and Risks). In a former mining tunnel, an *NP*91 explosive charge – either suspended at mid-height or put on ground – was detonated. The geometry and dimensions of the tunnel are shown in Fig. 12, and the explosive charge is located 29.50 m from the tunnel's closed end.

In order to determine the TNT equivalent factor of *NP*91, four series of trials were performed in free-field configuration. The corresponding weight of the tested charges, located on the ground, was: 25 *g*, 50 *g*, 100 *g* and 215 *g*. The explosive was formed into a hemisphere and detonated remotely. In order to assess the reproducibility of the data, the same series was repeated at least twice for each weight of the explosive charge. The uncertainty was found to be less than 10%. The measured pressures ranged between 26 mbar and 1180 mbar. Based on the maximum pressure effect [16–18], the TNT equivalence factor was found to be 1.18, where the fit has a correlation coefficient of 0.9089.

Fig. 13 shows the distribution of the maximum overpressure peak recorded at the different gauge positions for trials involving three explosive charges (150 *g*, 300 *g* and 600 *g*) located on the ground and another one (300 *g*) suspended at the tunnel's symmetry axis. Table 3 provides the transition zone provided by experimental results compared to the present predictions applying Eq. (8). Clearly, the predictions match the experimental results quite well. In addition, the ratio of the transition mean distance for $m_c = 300\,g$ along the tunnel symmetry axis to a charge of the same weight and quantity on the ground is about 1.12. This value is quite close to the predicted coefficient $\left((4/3)/\sqrt[3]{\beta}\right)^{13/9} = 1.14$ reported in Section 4.

6. An application

In order to illustrate its relevance, the damage estimation method proposed in Section 3 was applied to Trial no. 2. Table 4 provides the maximum overpressure peaks recorded at different gauge positions and the corresponding predicted values. In the trials, the transition distance Z_{Trans} could not be determined at *a priori*. Therefore, the position of the transition distance can be determined only within an interval of two successive gauges where the overpressure slope (in log–log scale) shows an abrupt change. Clearly, the predictions fit reasonably well with experimental results, both in the free-field and quasi-one-dimensional propagation regions. Any discrepancies may be explained by measurement uncertainty and by the fact that the one-dimensional propagation model proposed does not take into account any viscous dissipation, which actually is more significant in these propagation regions. Thus, the results obtained suggest the suitability of the proposed damage estimation method.

7. Conclusion

In this article, a parametric study was conducted in order to determine the behavior of the blast wave in a tunnel due to the explosion of condensed materials. In the region near the blast source, the wave propagates essentially like a free-field wave. As the wave interacts with the tunnel walls, the propagation pattern changes into a driven wave, behaving like a quasi-one-dimensional wave. For each likely propagation pattern, laws relating the maximum overpressure experienced to the distance were given, though the applicability limits of each of those laws were not given.

Using an appropriate numerical test bench, the explosion of different quantities of centered TNT charges inside a tunnel was simulated. The ratio of the equivalent TNT explosive quantity to the tunnel's hydraulic diameter was taken as the parameter defining the confinement of the explosion. The transition reduced distance variations suggested a correlation law depending only upon this confinement parameter. Using geometric considerations only, this correlation law was generalized for an explosion source near the tunnel wall and near a corner in the tunnel. The results given by the correlation law were successfully compared to experimental data for explosions inside tunnels.

The proposed damage estimation method was also validated by comparison with experimental measurements. This method could be very useful for assessing with relative good confidence the pressure undergone and the damage level provoked by an explosion, provided are known the quantity and the material of the explosive and the tunnel's characteristic cross-sectional area.

Although the proposed law and method will already increase the knowledge about the vulnerability to explosion risks in underground structures, the method presented here can be improved by integrating the viscous dissipation essentially due to tunnel wall friction, which can influence the blast wave amplitude and arrival time.

Acknowledgment

This research was carried out for the EGSISTES project, supported by the French National Research Agency (ANR), under contract no. ANR-06-SECU-004-02.

References

[1] W.E. Baker, P.A. Cox, P.S. Westine, J.J. Kulesz, R.A. Strehlow, Explosion Hazards and Evaluation. Fundamental Studies in Engineering, Elsevier, New York, 1983.
[2] C. Mills, The design of concrete structures to resist explosions and weapons effects, in: 1st Int. Conf. Hazard. Prot., Edinburgh, UK, 1987.
[3] H.L. Brode, Blast waves from a spherical charge, Phys. Fluids 2 (2) (1959) 217–229.
[4] J. Henrych, The Dynamics of Explosion and Its Use, Elsevier Press, Amsterdam, 1979.
[5] W. Taylor, Blast wave behavior in confined regions. Prevention of and protection against explosion of munitions, fuels and other hazardous mixtures, Ann. NY Acad. Sci. 152 (1968) 357–361.
[6] D. Curran, Underground storage of ammunition – experiments concerning accidental detonation in an underground chamber, Tech. Rep., Norwegian Defense Research Establishment, 1996.
[7] A. Smith, M. Sapka, Detonation wave propagation in underground mine entries.
[8] M. Silvestrini, B. Genova, F. Leon Trujillo, Energy concentration factor. a simple concept for the prediction of blast propagation in partially confined geometries, J. Loss Prevent. Proc. 22 (2009) 449–454.
[9] G. Kinney, Explosive Shocks in Air, MacMillan, London, 1962.
[10] S. Trélat, Impact de fortes explosions sur les bâtiments représentatifs d'une installation industrielle, PhD Thesis, Université d'Orléans, 2006.
[11] G. Kinney, K. Graham, Explosive Shocks in Air, 2nd ed., Springer-Verlag, New York, 1985.
[12] C. Mader, Numerical Modeling of Explosives and Propellants, 2nd ed., Univ. California Press, 1998.
[13] A. Benselama, M.-P. William-Louis, M. François, A 1D–3D mixed method for the numerical simulation of blast waves in confined geometries, J. Comput. Phys. 228 (2009) 6796–6810.
[14] B. van Leer, Towards the ultimate conservative scheme. V. A second-order sequel to Godunov's method, J. Comput. Phys. 32 (1) (1979) 101–136.
[15] F. Deister, E. Waymel, F. Hirschel, F. Monnoyer, Self-organizing hybrid cartesian grid generation and application to external and internal flows, Numer. Flow Sim. III, in: E.H. Hirschel (Ed.), Notes on Numerical Fluid Mechanics and Multidisciplinary Design vol. 82, 2002, pp. 18–29.
[16] E. Esparza, Blast measurments and equivalency for spherical charges at small charges at small scaled distances, Int. J. Impact Eng. 4 (1) (1986) 23–40.
[17] S. Formby, R. Wharton, Blast characteristic and TNT equivalence values for some commercial explosives detonated at ground level, J. Hazard. Mater. 50 (1996) 183–198.
[18] R. Wharton, S. Formby, R. Merrifield, Air blast TNT equivalence for a range of commercial blasting explosives, J. Hazard. Mater. 79 (2000) 31–39.